Journal of Southeast University (English Edition) Vol. 28, No. 4, pp. 457 - 463 Dec. 2012 ISSN 1003—7985

Analysis of mechanical performance of braided esophageal stent structure and its wires

Ni Xiaoyu[1] Wang Guo[2] Long Zhihong[2] Pan Changwang[3]

([1]School of Mechanical and Electronic Engineering, Nanjing Forestry University, Nanjing 210037, China)
([2]Jiangsu Key Laboratory for Design and Manufacture of Micro-Nano Biomedical Instruments, Southeast University, Nanjing 211189, China)
([3]Micro-Tech (Nanjing) Co., Ltd, Nanjing 210069, China)

Abstract: This paper aims to find the relationship between the structural parameters and the radial stiffness of the braided stent and to understand the stress distribution law of the wires. According to the equation of the space spiral curve, a three-dimensional parametrical geometrical model is constructed. The finite element model is built by using the beam-beam contact elements and 3D beam elements. The constituent nitinol wires are assumed to be linear elastic material. The finite element analysis figures out that the radial stiffness of the stent and the stress distribution of the wires are influenced by all the structural parameters. The helix pitch of the wires is the most important factor. Under the condition of the same load and other structural parameters remaining unchanged, when the number of wires is 24, the stress of the wire cross-section is at the minimum. A comparison between the vitro experimental results and the analytical results is conducted, and the data is consistent, which proves that the current finite element model can be used to appropriately predict the mechanical performance of the braided esophageal stents.

Key words: braided esophageal stent; finite element; mechanical performance; radial stiffness; wire
doi: 10.3969/j.issn.1003 - 7985.2012.04.015

The medical stent has been widely used in interventional medical engineering. The safety and reliability of the stent play the fundamental roles of stents. Vascular stents are generally made by laser engraving[1-3], nonetheless, most of the esophageal stents and other non-vascular stents are braided using nitinol wires. The braided stent consists of multi-clockwise and counterclockwise directional, cross-cutting spiral wires. According to different implantation locations, the braided esophageal stent can be divided into cup-spherical-shaped form, double spherical-shaped form, double horn-shaped form and other forms. The braided stent has the following characteristics: 1) The wires in the junction points can rotate and slip relatively because the grid nodes of the stent structure are not welded. Thus, the stent bending performance can be adapted to the bending deformation of the body cavity shape. 2) The nitinol wire of the stent maintains original surface conditions and uniform size because the tubular stent is constructed by manual fabrication using only one nitinol wire. 3) The stent structure is less prone to fatigue because no stress concentration points exist in nitinol wires. 4) The covered stent implanted in the esophagus can inhibit the growth of the tumor and cover the fistula. For this reason, the market demand of the braided stent is increasing.

Generally, the braided stent is safe and reliable to meet the clinical demands, depending on the stent radial strength and fatigue life. For the braided stents, some scholars have computed the stent radial force[4] and fatigue life[5] and optimized the braided stent structure by using the finite element method[6]. Jedwab and Clerc[7] developed an analytical model with the main assumption that the stent acts as a combination of a number of independent open-coiled helical springs with ends fixed against rotation, and each spring with no friction or steric obstruction. Kim et al.[8] developed a mechanical model for designing self-expandable stents. However, they focused on the compressive behavior, hysteresis behavior and the braiding technology of braided stents.

The mechanical properties of the wires during the loading process have a decisive impact on the whole braided stent structure. For example, the fatigue lives of the stents completely depend on the stress of the wires. However, few studies of the braided stents have been involved in the mechanical properties of the wires inside the braided stent. To the best of our knowledge, no literature has been reported on the finite element analyses of the stress, the deformation and the contact pressure for the braided nitinol wires. The purpose of the present study is to establish a complete contact analytical model for braided stents and to study the radial stiffness of the stents, the stress distribution of wires and the deformation law of the

Received 2012-07-31.
Biography: Ni Xiaoyu (1975—), female, doctor, associate professor, xyni_luck@163.com.
Foundation items: The National Natural Science Foundation of China (No. 51005124), the Opening Foundation of Jiangsu Key Laboratory for Design and Manufacture of Micro-Nano Biomedical Instruments (No. JSNB-2009-1-1).
Citation: Ni Xiaoyu, Wang Guo, Long Zhihong, et al. Analysis of mechanical performance of braided esophageal stent structure and its wires [J]. Journal of Southeast University (English Edition), 2012, 28(4): 457 - 463. [doi: 10.3969/j.issn.1003 - 7985.2012.04.015]

braided stents using the finite element method with various structural parameters.

In addition, the experimental results obtained by the testing method proposed in Ref. [4] are compared with the analytical results.

1 Materials and Methods

1.1 Geometrical modeling

An esophageal stent made by Micro-Tech (Nanjing) Co., Ltd is taken as an example to create the geometrical model of the stent (see Fig. 1). Based on the characteristics of the braided stents and nitinol wires woven in space spiral curves, setting the *Z*-axis along the longitudinal direction, the *X*-axis as the stent radial direction, the *Y*-axis as the stent circumferential direction, using the secondary development language APDL (ANSYS parameter design language) of the finite element software ANSYS, the parametric geometrical model of the braided stent is built. A preprocessor program is developed using the APDL, including three steps as follows.

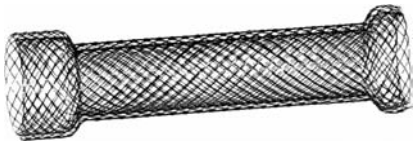

Fig. 1 Photograph of cup-spherical-shaped braided stent

In the first step, one helix in the clockwise rotation is generated by controlling the coordinate of every key point of the helix, and then the counterclockwise rotation line from the clockwise rotation line is generated by symmetry reflection. The coordinate of every key point can be expressed as

$$x_i = \frac{D}{2}\cos\theta_i,\ y_i = \frac{D}{2}\sin\theta_i,\ z_i = \frac{S}{2\pi}\theta_i$$
$$\theta_i = \frac{2\pi L}{SN_c}i;\ i = 1, 2, \ldots, N_c \quad (1)$$

where D is the diameter of the stent; L is the length of the stent; S is the helix pitch; N_c is the the total count of all the key points, which is decided depending on the demand of the modeling accuracy; i is the number of the key points.

In the second step, the *X* coordinate of the intersection points of two cross-cutting lines are modified by adjusting the *X* coordinate. The other lines are generated by copying in a circumferential direction. However, the clockwise rotate wires and the counterclockwise rotate wires may diverge at one end of the stent because of different braiding parameters. In the last step, by program testing and controlling, a curve is generated automatically to connect the two discrete points.

The geometrical model is shown in Fig. 2. The wire diameter d, the stent diameter D and the stent length L are the geometrical parameters. The number of wires N and the pitch of wires S are the braiding parameters. In the weaving process, the helix angle β is one of the most directive control parameters, which is the angle between the nitinol wire and the stent longitudinal direction. β is related to S and it can be determined by

$$\tan\beta = \frac{\pi D}{S} \quad (2)$$

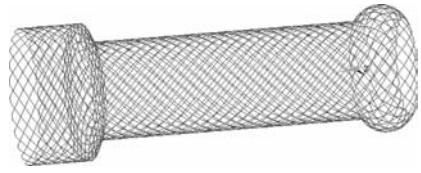

Fig. 2 Geometrical model of cup-spherical-shaped braided stent

According to Eq. (2), S and β have an inverse correlation, so the greater the S, the smaller the β will be. S is one of the parameters controlling the grid density of the stent structure, which is a major factor affecting the stiffness of the stent, and the radius of the curvature of helix ρ_r is an important factor affecting the torsion deformation of the nitinol wires inside the stent and it can be expressed by

$$\rho_r = \frac{\sqrt{D^2\pi + S^2}}{2\pi} \quad (3)$$

According to Eq. (3), it demonstrates that the greater the S, the greater the ρ_r will be.

1.2 Finite element model

It is not necessary to build a three-dimensional solid model for the braided esophageal stent because the wire diameter is small relative to the size of the stent structure. When the stent is implanted into a body cavity, under various loads, such as the radial pressure of the cavity, the wires inside the stent will produce tensile, bending and torsion deformation; therefore, the Beam189 or Beam188 element (Beam189 and Beam188 are defined as beam elements in finite element commercial software ANSYS) can be chosen to simulate the wires because the element type is based on the Timoshenko beam theory. The geometrical model can be meshed to form the finite element model, but junctions of two wires are not considered, which requires using contact elements to deal with. The finite element model of the braided stent is shown in Fig. 3. The initial values of the geometrical and braiding parameters and the material properties of the nitinol wires are listed in Tab. 1.

1.3 Contact condition

The relative rotation and relative slippage will occur at the intersections of the interwoven wires under certain loads. The stent wires are not independent of each other

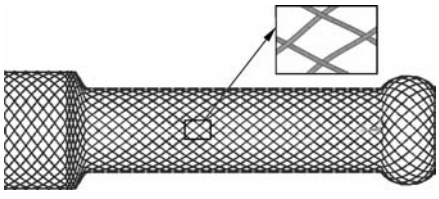

Fig. 3 Finite element model of braided stent

Tab. 1 Structural parameters and material properties[9]

Type	Parameter	Value
Braiding parameters	Initial number of wires N	24
	Initial helix pitch S/mm	60
Geometrical parameters	Wire diameter d/mm	0.2
	Initial stent length L/mm	80
	Initial diameter of stent D/mm	20
Material properties	Young's modulus E/GPa	83
	Yield strength σ_s/MPa	195 to 690
	Poisson ratio	0.3
	Density ρ/(kg · m^{-3})	6 450

because of friction, so considering the junction of two wires as welded or as free or as coupling some degrees of freedom is unreasonable. To simulate the mechanics properties of the true structure correctly, the beam-beam contact elements (CONTA176 and TARGET170 are also defined as contact elements in the finite element commercial software ANSYS) are selected, and then a flexible-to-flexible and symmetric contact model is created, as shown in Fig. 4. In this study, the frictional coefficient is set to be 0.15.

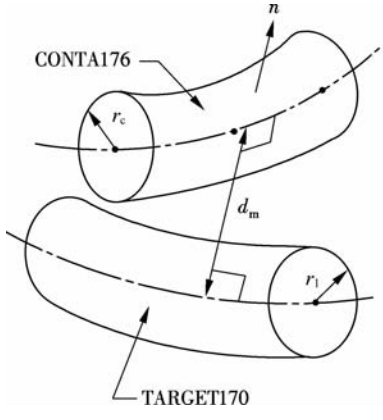

Fig. 4 Contact model

Due to the nonlinear contact analysis problem of the stent structure, the contact properties, including normal penalty stiffness, penetration tolerance etc., must be set correctly to ensure convergence of computing.

Contact is detected when two circular beams touch or overlap each other. The non-penetration condition for beams with a circular cross section can be defined as

$$g = d_m - (r_c + r_t) \leqslant 0 \tag{4}$$

where r_t and r_c are the radii of the cross sections of the beams on the contact and target sides, respectively, and d_m is the minimal distance between the two beams, which also determines the contact normal direction. Contact occurs for negative values of g. The element real constants are used to define the target radius r_t and the contact radius r_c on the basis of the wire diameter. For example, if the wire diameter is $d = 0.2$ mm, then the minimum distance between the two beams is $d_m = 0.2$ mm, so the target radius r_t and the contact radius r_c are set to be 0.101 mm, respectively.

1.4 Boundary condition and nonlinear solution control

The stent in the body cavity does not produce rotation and sliding because the stent cylindrical surface of the stent bears the balance compression from the cavity wall. Therefore, these external constraints can be simplified to be the boundary conditions for computing as follows: 1) Apply an axial zero displacement (UZ = 0) constraint on the one distal end of the stent and let the other end be free; 2) Apply the ROTZ axis rotation constraint; 3) Apply the radial non-zero displacement (UX) constraint to the outer nodes of the stent, which represents that the stent bears radial compression. The value of the UX is set according to the actual radial compression of the stent. In this article, the radial compression is about 30% of the original diameter of the stent. The boundary condition coordinate system is the same as the modeling coordinate system, which is described in section 2.1. These boundary conditions can ensure that the stent does not produce any rigid body motion including axial displacement and rotation around the Z axis, but allows one distal end of the stent to be free to produce axial elongation, and imitate the actual stent behavior as much as possible.

As the radial compression reaches 30% of the original diameter of the stent, the deformation of the stent structure belongs to the nonlinear large deformation problem. At the same time, the beam-beam contact is also a nonlinear problem because nonlinearity exists in the contact interface, which will change with the contact area size, location and contact state. Taking into account the significant changes of the contact state and penetration during the linear iterative process, the augmented Lagrangian method is taken as the contact algorithm and the automatic bisection is taken as the time-step control method to ensure the convergence of the nonlinear static analysis.

2 Results and Discussion

2.1 Stress of stent and wires and rule of deformation

The whole stent structure will generate the uniform axial elongation and radial deformation when the stent bears uniform radial compression. Because the nitinol wires of the stent are interwoven space spiral lines, they can produce the combined deformation, including tensile, bending and torsion deformation. Under the same boundary

conditions, the analytical results with different structural parameters are obtained (see Tabs. 2, 3 and 4). According to these results, the deformation law of stents and the stress distribution of wires can be obtained. The stress values of the wires in the middle part of the stent are listed in Tabs. 2, 3 and 4.

Tab. 2 The analytical results of different pitches of wires

N	S/mm	d/mm	σ/MPa	τ/MPa	ΔL/mm	p_c/MPa
24	30	0.2	260.690	96.129	43.924	0.189 7
24	35	0.2	236.791	82.497	34.752	0.174 7
24	40	0.2	215.085	70.761	27.631	0.169 8
24	45	0.2	209.118	60.750	22.799	0.151 1
24	50	0.2	177.060	52.216	18.965	0.143 2
24	55	0.2	162.328	44.991	15.967	0.125 3
24	60	0.2	148.209	38.871	13.677	0.114 8
24	70	0.2	129.915	30.672	10.408	0.112 0
24	80	0.2	108.267	23.448	8.054	0.089 9

Tab. 3 The analytical results of different numbers of wires

N	S/mm	d/mm	σ/MPa	τ/MPa	ΔL/mm	p_c/MPa
18	60	0.2	154.411	40.960	13.667	0.073 4
20	60	0.2	154.403	40.880	13.796	0.088 5
22	60	0.2	154.501	40.794	13.921	0.103 6
24	60	0.2	148.209	38.871	13.677	0.114 8
26	60	0.2	154.554	40.604	13.782	0.130 3
28	60	0.2	153.506	40.497	13.897	0.152 5

Tab. 4 The analytical results of different wire diameters

N	S/mm	d/mm	σ/MPa	τ/MPa	ΔL/mm	p_c/MPa
24	60	0.16	145.591	36.768	13.677	0.102 7
24	60	0.18	146.391	37.909	13.677	0.103 4
24	60	0.20	148.295	38.871	13.677	0.114 8
24	60	0.22	147.950	38.821	13.677	0.126 2
24	60	0.24	154.664	40.589	13.677	0.157 9

Notes: σ is the equivalent stress of wires; τ is the shear stress of wire cross section; and ΔL is the axial elongation of the stent.

According to the results in different groups, with the increase in N and d and the decrease in the pitch of wires, the equivalent stress and the shear stress of the stent structure will increase. Accordingly, with the increase in N and d and the decrease in S, the stiffness of the stent structure will increase. However, when $S = 40$ mm, the equivalent stress is 215.058 MPa, but when $S = 80$ mm, the equivalent stress is only 108.267 MPa. The value of equivalent stress is decreased by 50%. Because the bigger the S, the smaller the curvature will be, which makes nitinol wires produce less torsion deformation, and then the torsion shear stress is naturally less. When S increases from 40 to 80 mm, the shear stress is decreased by nearly 30%. Compared to S, d and N have less impact on the stress.

One important point worthy to be noted is that when N is 24 and the other parameters are the same, the equivalent stress and the shear stress are at a minimum. The stress law is consistent with the results obtained by other modeling methods, such as coupling nodes or welding nodes in the crossing of wires. If the stent fatigue life directly links to the equivalent stress, the stent fatigue life will reach the maximum when N is 24. Hence, $N = 24$ can be the best choice for the stent fatigue life when other structural parameters are the same.

From Tab. 2, it can be clearly observed that when S increases from 30 to 80 mm, the axial elongation is decreased by approximately 20%. From Tab. 3, the axial elongation does not change significantly with N increasing. From Tab. 4, d has no influence on the axial elongation. The axial elongation of the stent causes the friction between the stent and the wall of esophagus, which causes tissue proliferation. Thus, it is necessary to control the axial elongation of the stent by selecting reasonable S to decrease the friction.

The contact pressure exists at the contact points of the cross-cutting wires. From Tabs. 2, 3 and 4, the contact pressure increases with N and d increasing and S decreasing. If the stent has a big enough ability to resist compression, the contact pressure will be larger. This may be because the frictional force between the crossing wires can help the stents to resist deformation. Obviously, all the structural parameters have an influence on the mechanical performance of stents, but S is the most important parameter.

To observe the stress distribution on the wires, the middle part of the cross-cutting wires of the stent is chosen and enlarged. Figs. 5, 6 and 7 show the equivalent stress, the axial stress and the shear stress of the nitinol wires inside the braided stents, respectively.

According to Figs. 5, 6, and 7, the beam cross section is an octagon rather than a circle due to using the circular solid cross section with eight divisions along the circumference and two divisions through the radius. The division number can be increased or decreased only when it meets the accuracy requirements in finite element analysis.

The stress and strain distributions of the wires are uneven, whereas they have similar distribution characteristics. In the stent radial direction, the stress on the cross-section distributes in a layered form. Since the nitinol wires are subjected to the combined deformation, the maximum equivalent stress occurs at the outer edge of the wires and the minimum equivalent stress occurs at the middle part of the wires. According to the material mechanics, the stress distribution law is reasonable.

Under the radial compression, the outer side of the wires in the radial direction of the stent bears compression; therefore, the axial stress is negative. On the inner side of wires, the axial stress is positive but the absolute value is the same (see Fig. 6). And owing to the fact that the shear stress is caused by torsion deformation and contact, the shear stress is not zero in the center point of the wire cross-sections. The maximum shear stress occurs

at the inner and the outer sides of the wires surfaces in the contact direction. The value is the same but the direction is opposite (see Fig. 7). The law of stress distribution is also consistent with the material mechanics.

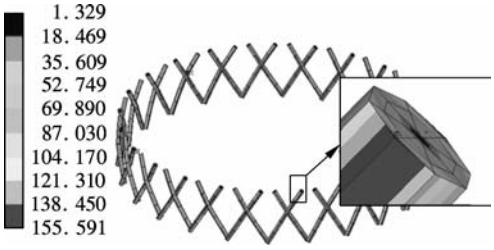

Fig. 5 Equivalent stress of nitinol wires in the middle part of the stent ($N=24$, $S=60$ mm, $d=0.16$ mm)

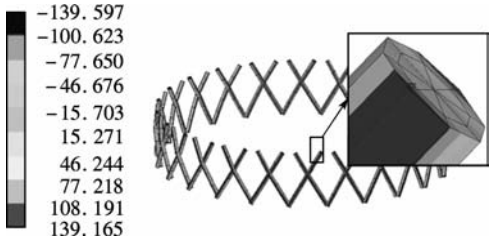

Fig. 6 Axial stress of nitinol wires in the middle part of the stent ($N=24$, $S=60$ mm, $d=0.16$ mm)

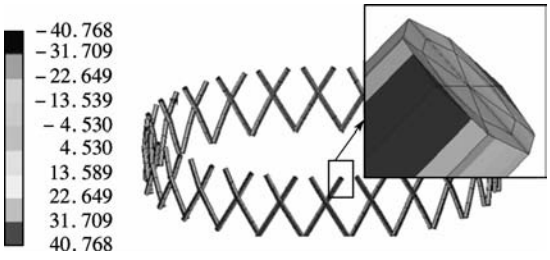

Fig. 7 Shear stress of nitinol wires in the middle part of the stent ($N=24$, $S=60$ mm, $d=0.16$ mm)

For other different structural parameters, the law of stress distribution is the same. Thus, other diagrams of the stress distribution of wires with different parameters are not displayed in this paper.

2.2 Radial stiffness of stent

The radial stiffness of the stent is the most important index by which to judge the mechanical properties of the stent structure. This is why it is necessary to analyze and perform experiments separately. According to the convergent result, the reaction force F_i on each node bearing a radial displacement constraint is summed, and then the radial force can be obtained. Based on the thin-wall cylinder theory, the radial stiffness K of the stent is

$$K = \frac{\sum F_i}{\pi(D_o - \Delta D)(L_o + \Delta L)} \tag{5}$$

where D_o is the original stent diameter; ΔD is the radial displacement of the stent; L_o is the original stent length; and ΔL is the elongation displacement of the stent.

A complete derivation of Eq. (5) presented in this section is summarized by Wang et al.[4] and Huang et al[10].

The test experiments of the radial stiffness of the stents and the comparison between the analytical data and the experimental data are conducted for verification. Fig. 8 illustrates the setup of the stent radial stiffness experiment, and the test method is described in detail in Ref. [4]. Three groups of stents with different structural parameters, including N (=16, 18, 20, 22, 24), S (=40, 50, 60, 70, 80 mm) and d (=0.16, 0.18, 0.20, 0.22, 0.24 mm) are tested. In the experiment, all the initial diameters of the test stents are set to be 20 mm and the radial compression is 30% of the initial diameters. The experimental results are obtained and shown in Tab. 5.

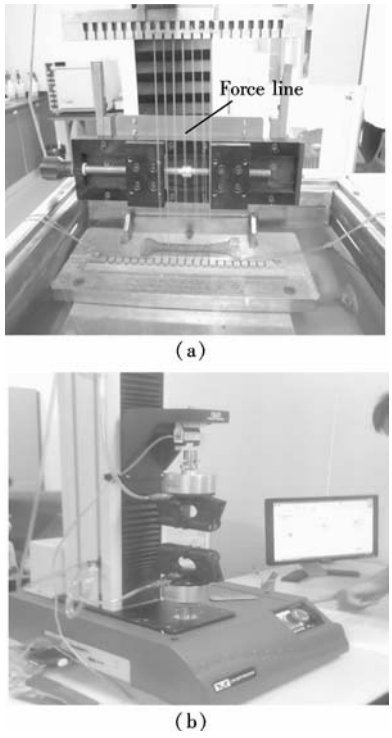

Fig. 8 Experimental setup for radial stiffness of stent. (a) Loading; (b) Data acquisition and analysis (INSTRON tensile machine)

Tab. 5 Experimental results

Group	Parameters	Radial stiffness/kPa
1	$S=60$ mm $d=0.2$ mm different N	1.949 ($N=20$) 2.004 ($N=22$) 2.382 ($N=24$) 2.867 ($N=26$) 3.126 ($N=28$)
2	$S=60$ mm $N=24$ different d	2.605 ($d=0.16$ mm) 3.203 ($d=0.18$ mm) 3.862 ($d=0.20$ mm) 5.282 ($d=0.22$ mm) 5.973 ($d=0.24$ mm)
3	$N=24$ $d=0.2$ mm different S	4.005 ($S=40$ mm) 2.564 ($S=50$ mm) 2.382 ($S=60$ mm) 1.799 ($S=70$ mm) 1.706 ($S=80$ mm)

In this test setup, the axial deformation of the stent can make the force lines (see Fig. 8(a)) tilt and no longer remain vertical because there is the friction between the stent and the force lines. Besides, the possible preloads of the force lines are unpredicted. Of course, there may be some other uncertainties; therefore, the experimental results may have large errors and instability. When $N = 24$, $d = 0.2$ mm and $S = 60$ mm, the value of the radial stiffness is greater in the second group than in the other two groups (see Tab. 5). The test setup will be improved in our follow-up work.

Figs. 9, 10 and 11 show the variation trend of the radial stiffness of stents with different parameters and exhibit the comparison between the experimental data and the analytical data. There is an exceedingly good agreement between experiment and analysis. However, the analytical results are smaller than the experimental results, which may be due to the errors of the experiment and the relevant assumptions in simulation.

Obviously, as S increases, the radial stiffness of the stent sharply decreases, especially, when S increases from 40 to 70 mm (see Fig. 9). From Fig. 9, it can be clearly observed that the radial stiffness decreases with the increase in the pitch of the wires. It can be concluded that S is the most important parameter to determining the radial stiffness of the braided stent.

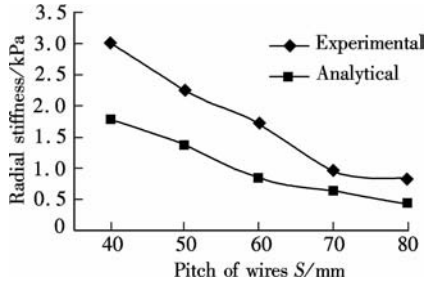

Fig. 9 The radial stiffness of stents vs. the pitch of wires

Although the experimental results are greater than the analytical results, the changing trends of the two lines are almost the same. More wires make the stent structure denser, and the radial stiffness increases (see Fig. 10). From Fig. 10, it can be clearly observed that the radial stiffness increases with the increase in the number of wires.

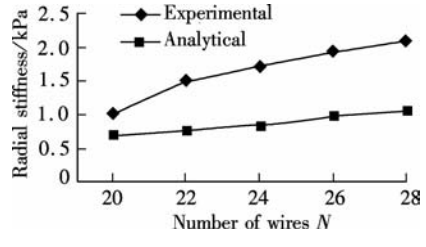

Fig. 10 The radial stiffness of stents vs. the number of wires

It can also be clearly observed that the experimental value increases sharply when d increases, while a relative plateau appears in the analytical value (see Fig. 11), which may be due to the frictional coefficient in simulation. From Fig. 11, it can be clearly seen that the radial stiffness increases with the increase in the wire diameter. A parametric study will be carried out to determine the proper frictional coefficient of the nitinol wires in our follow-up simulations.

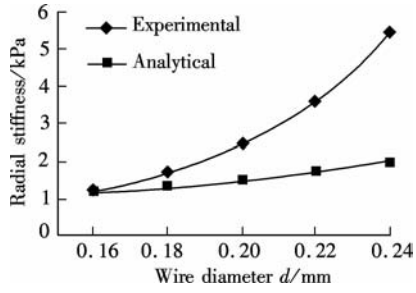

Fig. 11 The radial stiffness of stents vs. the diameter of wires

3 Conclusion

In this study, the geometrical model for braided stents can be quickly built, which can be used to investigate the mechanical behavior of stents with different structural parameters. Based on the analytical and experimental results, the wires inside stents are not totally independent and cannot be regarded as some simple helixes or simple springs because contact pressure (see Tabs. 2, 3 and 4) can exhibit the common action at the cross-cutting points.

The law of stress distribution and deformation of the stents is obtained. Under the same radial compression, S has the largest influence on the axial elongation, the equivalent stress and the shear stress of the stents. It is noted that in the case of $N = 24$, the stress of wires is isolated, which is immensely important to the fatigue life of braided stents.

In the purpose of obtaining a better stent design and preferably meeting the clinical application, it is necessary to know the comprehensive performance of stents by means of using multi-objective optimization. Assuredly, the corresponding numerical analysis and experiments are extremely essential for coated stents.

References

[1] Li N, Zhang H W, Ouyang H J. Shape optimization of coronary artery stent based on a parametric model[J]. *Finite Elements in Analysis and Design*, 2009, **45**(6/7): 468 - 475.

[2] Li N, Zhang H W. Numerical research on longitudinal flexibility of a coronary stent[J]. *Chinese Journal of Computational Mechanics*, 2011, **38**(3): 309 - 314. (in Chinese)

[3] Wang Y X, Yi H, Ni Z H, et al. Research on biomechanical characteristic of medical vascular stent[J]. *Journal of Southeast University: Natural Science Edition*, 2005, **35**(2): 216 - 221. (in Chinese)

[4] Wang G, Ni Z H, Ni X Y, et al. Radial support proper-

ties of esophagus stent[J]. *Journal of Southeast University: Natural Science Edition*, 2011, **41**(5): 987 - 991. (in Chinese)
[5] Ni X Y, Ni Z H, Pan C W. Analysis on fatigue life of esophagus stent based on finite element[J]. *Journal of Southeast University: Natural Science Edition*, 2009, **39**(5): 919 - 922. (in Chinese)
[6] De Beule M, Van Cauter S, Mortier P, et al. Virtual optimization of self-expandable braided wire stents[J]. *Med Eng Phys*, 2009, **31**(4): 448 - 53.
[7] Jedwab M R, Clerc C. A study of the geometrical and mechanical properties of a self-expanding metallic stent-theory and experiment[J]. *Journal of Applied Biomaterials*, 1993, **4**(1): 77 - 85.
[8] Kim J H, Kang T J, Yu W R. Mechanical modeling of self-expandable stent fabricated using braiding technology [J]. *J Biomech*, 2008, **41**(15): 3202 - 3212.
[9] Zheng Y F, Zhao L C. *Biomedical nitinol*[M]. Beijing: Science Press, 2004:39. (in Chinese)
[10] Huang Y P, Fan Z N, Li Y H, et al. Study for medical endoprosthesis mechanics efficiency and test method [J]. *China Medical Device Information*, 2008, **14**(10):49 - 53. (in Chinese)

编织型食管支架结构及其丝线的力学性能分析

倪晓宇[1] 王 果[2] 龙志红[2] 潘长网[3]

([1] 南京林业大学机械电子工程学院,南京 210037)
([2] 东南大学江苏省生物医疗器械设计与制造重点实验室,南京 211189)
([3] 南京微创医学科技有限公司,南京 210069)

摘要:旨在找出支架结构参数与支架径向刚度之间的关系并了解支架变形及丝线上的应力分布规律.按照空间螺旋曲线方程创建几何模型,用梁-梁接触单元和三维梁单元建立有限元模型,并定义丝线为线弹性材料.有限元分析结果显示支架结构径向刚度及丝线上的应力分布与支架的各个结构参数都相关,其中丝线螺距对其影响最大.在相同载荷作用下,当丝线头数是24且支架的其他结构参数都不变时,丝线横截面上的应力最小.最后,将体外实验结果与分析结果进行比较,数据规律具有一致性,可以证明该有限元模型能够用于近似预测编织型食管支架的相关力学性能.

关键词:编织型食管支架;有限元;力学性能;径向刚度;丝线
中图分类号:R318